Application of H_2/H_∞ and Dynamic Inversion Techniques to Aircraft Landing Control

Romulus Lungu[1], Mihai Lungu[2]

[1]University of Craiova, Faculty of Electrical Engineering, 107 Decebal Blvd., Craiova, Romania, romulus_lungu @yahoo.com
[2]University of Craiova, Faculty of Electrical Engineering, 107 Decebal Blvd., Craiova, Romania, Lma1312 @yahoo.com

The paper focuses on the aircraft automatic control in longitudinal plane, during landing, taking into account the sensor errors and disturbances. Aircraft auto-landing is achieved by combining the mixed H_2/H_∞ and the dynamic inversion control techniques and by using an optimal observer, the geometry of landing, and two reference models. The general control law will consist of a guidance component for the commanded landing trajectory (calculated by using the dynamic inversion approach) and an optimal component which will be designed by means of a mixed H_2/H_∞ technique for the cancel of the sensor errors and other disturbances in the system. The theoretical results are validated by numerical simulations for the landing of a Boeing 747; the simulation results are very good, Federal Aviation Administration accuracy requirements for best category being met.

Key words: Aircraft landing, H_2/H_∞ control, Dynamic inversion, Glide slope, Flare

1. Introduction

The control of aircraft during landing is a problem of both theoretical and practical interest because it is well known that landing is the most challenging among all flight phases of aircraft. During landing, accidents are more likely to happen because the aircraft flies at a considerable low altitude and low speed and because of wind turbulences, wind shears, measurement noises, and so on [1]; that is why, robustness to these disturbances is the main challenge in the design of Automatic Landing Systems (ALSs). Furthermore, these ALSs must consistently control an aircraft to an accurate touchdown point and a smooth touchdown to prevent its damage. In the design process, one can use different conventional control laws as: proportional-derivative (PD), proportional-integral (PI), proportional-integral-derivative (PID) for the altitude and descent velocity control [2-5], PD or PID conventional laws for the pitch angle and pitch rate control, as well as different laws based on the state vector, dynamic inversion concept, with command filters, dynamic compensators, and state observers [1, 6-8]. The PID controllers designed for landing are easy to software implement, but these controllers have not satisfying performances and robustness, especially in the cases of flight dynamics affected by disturbances and uncertainties [9]; therefore, to increase the robustness of the landing controllers and the safety of landing, these controllers can be replaced by robust controllers based on intelligent concepts for automatic landing; they used the optimal synthesis H_2, H_∞, H_2/H_∞ [5, 10], the adaptive synthesis based on dynamic inversion theory and neural networks theory [11, 12], quantitative feedback theory [13], sliding mode control [14], linear quadratic optimal control (LQR/LQG), structured singular value μ-synthesis, or fuzzy techniques [15]. Feed-forward neural networks with back propagation learning algorithm have also been used [8], the main drawback of such systems being that the neural networks require a priori training on normal and faulty operating data. In [16] the feedback linearization method has been used for nonlinear control in the design of an automatic landing system; unfortunately, the paper presents limited insight into the performance of simulations of this controller and no tests are performed outside of these simulations. In the work of Singh and Padhi [4] a nonlinear control has been designed using the dynamic inversion approach for the automatic landing of unmanned aerial vehicles along with associated path planning. In the research area of optimal synthesis, Shue and Agarwal [9] have developed a mixed technique for the H_2/H_∞ control of landing, while Ochi and Kanai [17] have used the H_∞ control technique to design an approach for aircraft automatic and landing. In these papers, the authors did not analyze the robustness of the designed controllers in the presence of sensor errors and external disturbances – issue which is considered in our paper.

This paper focuses on the automatic control of aircraft in the longitudinal plane, during landing, by using the H_2/H_∞ technique, the dynamic inversion method, the geometry of landing, and an optimal observer, taking into consideration the errors of the sensors and other different disturbances; thus, our aim is to design a new landing flight control system which cancels the negative effect of disturbances and sensor errors and which can be used with good results when the number of sensors is smaller than the number of states. According to this paper's authors, little progress has been reported for the landing flight control systems in the longitudinal plane (using the H_2/H_∞ control and the dynamic inversion) handling all the above presented problems; this motivates the present study.

The ALS designed in this paper represents an improved version of the automatic landing system designed in [6] and it differs from other similar automatic landing systems from the specialty literature. Our new automatic landing system has some additional elements with respect to the one presented in [6]: 1) the mixed H_2/H_∞ optimization formulation is used instead of H_∞ optimization approach which deals with bounded exogenous signals; 2) an optimal observer – used for the estimation of the aircraft state in the presence of sensor errors and external disturbances; 3) a subsystem based on the dynamic inversion technique

providing one of the two components of the mixed H_2/H_∞ control law; 4) a subsystem which models the geometry of landing providing the reference value of aircraft pitch angle; 5) two reference models providing the desired pitch angle, velocity on the landing curve, and their derivatives up to relative degrees of the system. The general control law consists of two components: 1) a guidance component $(\bar{\boldsymbol{u}})$, for the commanded landing trajectory, calculated by using the dynamic inversion approach; 2) an optimal component $(\hat{\boldsymbol{u}})$ – designed by means of a mixed H_2/H_∞ technique, that must cancel the sensor errors (biases) and other disturbances in the system. The calculation of $\bar{\boldsymbol{u}}$ differs from the one presented in [6] especially by a greater degree of generality, applicability, and simplicity; the control law presented in [6] consists of separating the controller in two subsystems: a stable one and an unstable one which must be stabilized separately, this leading to a more complicated design procedure.

The H_2/H_∞ control provides robust stability with respect to the uncertainties caused by sensor errors and other disturbances, while the dynamic inversion provides good precision tracking by generating a feedforward command. These techniques are combined and a robust automatic landing system is obtained. The weights of the H_2 and H_∞ control techniques within the robust H_2/H_∞ controller are adjusted such that the aircraft accurately tracks the desired trajectory during landing. By adding an optimal observer and two reference models providing the desired pitch angle and longitudinal velocity, one obtains a new automatic landing system which is very suited for landing control in the longitudinal plane.

2. Aircraft Dynamics and Landing Geometry

2.1. The geometry of landing

There are three phases in a typical landing procedure: initial approach, glide slope, and flare [18]. During initial approach, the pilot descends from the cruise altitude to an altitude of approximately 420 m above the ground for heavy aircraft or less than 420 m for light aircraft. The pilot then positions the airplane so that the airplane is on a heading towards the runway centerline. As the airplane descends along the glide slope path, its pitch, attitude, and speed must be controlled; the aircraft maintains a constant speed along the flight path. The descent rate, for a Boeing 747, must be about 3 m/s and the pitch angle is between -5 to 5 degrees. As the airplane descends to 7-30 m above the ground (the maximum value is for Boeing 747), the slope angle control system is disengaged and a flare maneuver is executed. The vertical descent rate is slightly decreased so that the landing gear may be able to dissipate the energy of the impact at landing. The pitch angle of the airplane is then adjusted, between 0 to 5 degrees for most aircraft, which allows a soft touchdown on the runway surface [12].

For the ***glide slope phase*** ($H \geq H_0$, H_0 – the altitude at which the glide slope phase ends and the second landing phase begins), the commanded (calculated) altitude H_c and the real altitude H are, respectively:

$$\dot{H}_c = V_0 \sin\gamma_c \cong V_0\gamma_c \,,\; \dot{H} = V_0 \sin\gamma \cong V_0\,\gamma = V_0\,(\theta - \alpha), \tag{1}$$

where $\gamma = \theta - \alpha$ is the real slope angle of the aircraft trajectory during landing, $\gamma_c = \theta_c - \alpha$ is the commanded value of this angle during the first stage of landing $(\gamma_c = -2.5\,\text{deg})$, V_0 – the nominal flight speed, α – aircraft attack angle, θ – aircraft pitch angle; because the slope angle, expressed in radians, has small values, the approximations $\sin\gamma \cong \gamma$ and $\sin\gamma_c \cong \gamma_c$ has been used in (1).

The dynamics associated to the ***flare phase*** $(H < H_0)$ has been presented in detail in [2]; the form of the calculated altitude H_c is $H_c = H_0 \exp(-t/\tau)$, with τ – the time constant that defines the exponential curve (flare landing phase). Let us consider H_{ref} – the altitude of the flare's final point (chosen below ground level such that the exponential trajectory associated to the flare intersects the runway in the desired point) [2]; therefore, the real altitude (H) is calculated with respect to H_{ref}, the relation between H and H_c being $H_c = H - H_{ref}$; by derivation of the above equation of H_c, we obtain:

$$\dot{H}_c = -\frac{1}{\tau}\underbrace{H_0 \exp(-t/\tau)}_{H_c} = -\frac{1}{\tau}H_c\,. \tag{2}$$

Taking into account that $H_c = H - H_{ref}$, the solution of the differential equation (2) is:

$$H_c = H_0 - \frac{1}{\tau}\int_0^{t_c}(H - H_{ref})\,dt\,, \tag{3}$$

where t_c is the flare's duration. Equation (3) expresses that, for the elimination of the tracking error associated to the altitude during the flare phase, one must use an ideal integrator after the tracking error, i.e. a state which expresses the integration of aircraft altitude [19]; this will be detailed latter in this section. Now, by using the equations (1) and (2), one can obtain the calculated value (reference value) of the aircraft pitch angle (θ_c) for the two stages of landing; it has the expressions:

$$\theta_c \cong \alpha + \frac{\dot{H}_c}{V_0} \cong \begin{cases} \alpha + \gamma_c\,, H \geq H_0\,, \\ \alpha + \dfrac{1}{V_0\tau}(H_{ref} - H), H < H_0\,. \end{cases} \tag{4}$$

2.2. Aircraft linearized dynamics in longitudinal plane

The dynamics used in this paper belongs to a Boeing 747; the linear model of the aircraft motion, in longitudinal plane, is described by the state equation [2, 3]:

$$\dot{\boldsymbol{x}} = A\boldsymbol{x} + B\boldsymbol{u} + G\boldsymbol{u}_w\,, \tag{5}$$

with $\boldsymbol{x} \in R^{4\times 1}$ – the state vector, $\boldsymbol{x} = \left[u\ \ w\ \ q\ \ \theta\right]^T$, $\boldsymbol{u} \in R^{2\times 1}$ – the command vector, $\boldsymbol{u} = \left[\delta_e\ \ \delta_T\right]^T$, while $\boldsymbol{u}_w$ is the vector of disturbances which is estimated by the equipment from aircraft's navigation system; in equation (5), u is the aircraft longitudinal velocity, w - aircraft vertical velocity, q – aircraft pitch angular rate, θ - aircraft pitch angle, while δ_e and δ_T are the elevator deflection and the engine command, respectively. Taking into account that w is much smaller than u, the aircraft velocity in longitudinal plane can be approximated as follows: $V = \sqrt{u^2 + w^2} \cong u$; thus, the nominal value of V is considered to be $V_0 \cong u(0) = u_0$. The matrices $A \in R^{4\times 4}, B \in R^{4\times 2}$ are, respectively [7]:

$$A = \begin{bmatrix} a_{11} & a_{12} & 0 & a_{14} \\ a_{21} & a_{22} & a_{23} & a_{24} \\ a_{31} & a_{32} & a_{33} & a_{34} \\ 0 & 0 & 1 & 0 \end{bmatrix}, B = \begin{bmatrix} b_{11} & b_{12} \\ b_{21} & b_{22} \\ b_{31} & b_{32} \\ 0 & 0 \end{bmatrix}. \tag{6}$$

If one extends the state vector $\boldsymbol{x}$ with two new states δ_e and δ_T (the outputs of the actuators), satisfying the equations: $\dot{\delta}_e = -\frac{1}{T_e}\delta_e + \frac{1}{T_e}\delta_{ec}, \dot{\delta}_T = -\frac{1}{T_T}\delta_T + \frac{1}{T_T}\delta_{Tc}$, then, the new state of the system becomes $\boldsymbol{x} = \left[\frac{u}{V_0}\ \ \frac{w}{V_0}\ \ q\ \ \theta\ \ \delta_e\ \ \delta_T\right]^T$, while the new command vector is $\boldsymbol{u} = \left[\delta_{ec}\ \ \delta_{Tc}\right]^T$; δ_{ec} and δ_{Tc} are the commands applied to elevator and to engines, respectively. Therefore, for $\boldsymbol{u}_w = 0$, the aircraft state equations are:

$$\begin{aligned} &\frac{\dot{u}}{V_0} = a_{11}\frac{u}{V_0} + a_{12}\frac{w}{V_0} + \frac{a_{14}}{V_0}\theta + \frac{b_{11}}{V_0}\delta_e + \frac{b_{12}}{V_0}\delta_T\,,\ \frac{\dot{w}}{V_0} = a_{21}\frac{u}{V_0} + a_{22}\frac{w}{V_0} + \frac{a_{23}}{V_0}q + \frac{a_{24}}{V_0}\theta + \frac{b_{21}}{V_0}\delta_e + \frac{b_{22}}{V_0}\delta_T\,, \\ &\dot{q} = V_0 a_{31}\frac{u}{V_0} + V_0 a_{32}\frac{w}{V_0} + a_{33}q + a_{34}\theta + b_{31}\delta_e + b_{32}\delta_T\,, \dot{\theta} = q, \dot{\delta}_e = -\frac{1}{T_e}\delta_e + \frac{1}{T_e}\delta_{ec}, \dot{\delta}_T = -\frac{1}{T_T}\delta_T + \frac{1}{T_T}\delta_{Tc}\,. \end{aligned} \tag{7}$$

Using the equation [2-4]: $w = V_0 \sin\alpha$ or $w \cong V_0\,\alpha$ for small values of the attack angle $(\sin\alpha \cong \alpha)$, for the aircraft control during the glide slope phase, the following state $\boldsymbol{x} \in R^{8\times 1}$ is chosen:

$$\boldsymbol{x} = \left[\frac{u}{V_0}\ \ \alpha\ \ q\ \ \theta\ \ \frac{H}{V_0}\ \ \frac{\dot{H}}{V_0}\ \ \delta_e\ \ \delta_T\right]^T, \tag{8}$$

Thus, to equations (7), one adds the differential equations associated to the variables H/V_0 and $\dot{H}/V_0$; these are:

$$\frac{\dot{H}}{V_0} \cong \theta - \alpha\,,\ \frac{\ddot{H}}{V_0} = -a_{21}\frac{u}{V_0} - a_{22}\alpha + \left(1 - \frac{a_{23}}{V_0}\right)q - \frac{a_{24}}{V_0}\theta - \frac{b_{21}}{V_0}\delta_e - \frac{b_{22}}{V_0}\delta_T\,; \tag{9}$$

the last one has been obtained by derivation with respect to time of the first equation (9), with $\dot{\alpha} = \dot{w}/V_0$ having the form (7).

Putting together equations (7) and (9), with the state vector (8), one obtains the matrices A and B:

$$A = \begin{bmatrix} a_{11} & a_{12} & 0 & \frac{a_{14}}{V_0} & 0 & 0 & \frac{b_{11}}{V_0} & \frac{b_{12}}{V_0} \\ a_{21} & a_{22} & \frac{a_{23}}{V_0} & \frac{a_{24}}{V_0} & 0 & 0 & \frac{b_{21}}{V_0} & \frac{b_{22}}{V_0} \\ V_0 a_{31} & V_0 a_{32} & a_{33} & a_{34} & 0 & 0 & b_{31} & b_{32} \\ 0 & 0 & 1 & 0 & 0 & 0 & 0 & 0 \\ 0 & -1 & 0 & 1 & 0 & 0 & 0 & 0 \\ -a_{21} & -a_{22} & \left(1 - \frac{a_{23}}{V_0}\right) & -\frac{a_{24}}{V_0} & 0 & 0 & -\frac{b_{21}}{V_0} & -\frac{b_{22}}{V_0} \\ 0 & 0 & 0 & 0 & 0 & 0 & -\frac{1}{T_e} & 0 \\ 0 & 0 & 0 & 0 & 0 & 0 & 0 & -\frac{1}{T_T} \end{bmatrix}, B = \begin{bmatrix} 0 & 0 \\ 0 & 0 \\ 0 & 0 \\ 0 & 0 \\ 0 & 0 \\ 0 & 0 \\ \frac{1}{T_e} & 0 \\ 0 & \frac{1}{T_T} \end{bmatrix}. \tag{10}$$

Denoting with $\boldsymbol{u}_w = \begin{bmatrix} u_g/V_0 & \alpha_g & q_g \end{bmatrix}^T$ – the vector of disturbances which are additionally introduced in the equations of the states $u/V_0, \alpha, q$, one yields the matrix G as follows:

$$G^T = \begin{bmatrix} a_{11} & a_{21} & V_0 a_{31} & 0 & 0 & -a_{21} & 0 & 0 \\ a_{12} & a_{22} & V_0 a_{32} & 0 & -1 & -a_{22} & 0 & 0 \\ 0 & a_{23}/V_0 & a_{33} & 1 & 0 & (1-a_{23}/V_0) & 0 & 0 \end{bmatrix}. \tag{11}$$

The first component of the vector $\boldsymbol{u}_w$ refers to the longitudinal gust, while the second one (α_g) refers to the vertical gust taking into account that $\alpha \cong w/V_0$ and, accordingly, $\alpha_g \cong w_g/V_0$; w_g is the speed of the vertical wind (disturbance).

For the aircraft control during flare, using the notation $\tilde{H}_c = \int_{t_o}^{t} H_c(\tau)\mathrm{d}\tau$ (t_0 – the time moment when the aircraft ends the glide slope phase and begins the flare phase), the following state $\boldsymbol{x} \in R^{8\times 1}$ is chosen: $\boldsymbol{x} = \begin{bmatrix} \frac{u}{V_0} & \alpha & q & \theta & \frac{H}{V_0} & \frac{\tilde{H}_c}{V_0} & \delta_e & \delta_T \end{bmatrix}^T$; matrix A is obtained with (10) modifying only the sixth line, while the matrix B is the same with the one in (10); thus, one gets:

$$A = \begin{bmatrix} a_{11} & a_{12} & 0 & \frac{a_{14}}{V_0} & 0 & 0 & \frac{b_{11}}{V_0} & \frac{b_{12}}{V_0} \\ a_{21} & a_{22} & \frac{a_{23}}{V_0} & \frac{a_{24}}{V_0} & 0 & 0 & \frac{b_{21}}{V_0} & \frac{b_{22}}{V_0} \\ V_0 a_{31} & V_0 a_{32} & a_{33} & a_{34} & 0 & 0 & b_{31} & b_{32} \\ 0 & 0 & 1 & 0 & 0 & 0 & 0 & 0 \\ 0 & -1 & 0 & 1 & 0 & 0 & 0 & 0 \\ 0 & 0 & 0 & 0 & 1 & 0 & 0 & 0 \\ 0 & 0 & 0 & 0 & 0 & 0 & -\frac{1}{T_e} & 0 \\ 0 & 0 & 0 & 0 & 0 & 0 & 0 & -\frac{1}{T_T} \end{bmatrix}, B = \begin{bmatrix} 0 & 0 \\ 0 & 0 \\ 0 & 0 \\ 0 & 0 \\ 0 & 0 \\ 0 & 0 \\ \frac{1}{T_e} & 0 \\ 0 & \frac{1}{T_T} \end{bmatrix}. \tag{12}$$

3. Design of the Control Laws and of the New ALS

3.1. Design of the H_2/H_∞ control law

The control of aircraft during the two landing phases is achieved in this section by designing a controller which uses both the H_2/H_∞ control and the dynamic inversion technique. The aim of the H_2 optimal control method is to improve the overshoot of the dynamic processes, while the H_∞ technique is a very good choice for the minimization of the disturbances effect on the system output variables (imposed as performance variables); thus, in this subsection, it will be obtained a mixed H_2/H_∞ control law which will be the first component $(\hat{\boldsymbol{u}})$ of aircraft's control law ($\boldsymbol{u}$).

To design the H_2/H_∞ control law, we choose the following output vector: $z = \begin{bmatrix} z_1 & z_2 \end{bmatrix}^T = \begin{bmatrix} \theta & u \end{bmatrix}^T$; the equations associated to the output variables to be controlled (aircraft pitch angle - θ and the longitudinal velocity - u) are:

$$z_1 = C_0 \boldsymbol{x} + D_{01}\boldsymbol{u},\ z_2 = C_1 \boldsymbol{x} + D_{11}\boldsymbol{u}, \tag{13}$$

For the first phase of landing (glide slope), taking into account the equations (1) and (8), one yields:

$$C_0 = \begin{bmatrix} 0 & 0 & 0 & 1 & 0 & 0 & 0 & 0 \end{bmatrix}, C_1 = \begin{bmatrix} V_0 & 0 & 0 & 0 & 0 & 0 & 0 & 0 \end{bmatrix}, D_{01} = \begin{bmatrix} c_1 & 0 \end{bmatrix}, D_{11} = \begin{bmatrix} 0 & c_2 \end{bmatrix}; \tag{14}$$

c_1 and c_2 are positive constants. Moreover, the equation of the measurement system can be written of the following form:

$$y = C\boldsymbol{x} + D_{22}e, \tag{15}$$

where $D_{22} = \bar{k}I_7$ ($\bar{k}$ – positive constant) is the matrix of weights associated to the vector containing the sensor errors [9]: $e = \begin{bmatrix} e_u & e_\alpha & e_q & e_\gamma & e_H & e_{\delta_e} & e_{\delta_T} \end{bmatrix}^T$, $y = \begin{bmatrix} u & \alpha & q & \gamma & H & \delta_p & \delta_T \end{bmatrix}^T$, while the matrix C is obtained by identification.

For the second phase of landing (flare), the equations (14) remain valid, but the forms of the vectors e and y become now: $e = \begin{bmatrix} e_u & e_\alpha & e_q & e_\theta & e_H & e_{\delta_e} & e_{\delta_T} \end{bmatrix}^T$, $y = \begin{bmatrix} u & \alpha & q & \theta & H & \delta_p & \delta_T \end{bmatrix}^T$; D_{22} has the same expression as the one in the case of the first landing phase, while the matrix C can be again easily obtained by identification.

It is known that the sensors (used to measure some important variables) have sometimes errors; for example, the most important errors of a gyro sensor are: 1) the bias; 2) the scale factor; 3) the calibration error of the scale factor; 4) the noise of the

sensor; 5) the sensibility to an acceleration applied along an arbitrary direction. The biases are the most severe for the control performance during landing. The general model of the gyro sensor is the one in [3]. In the software implemnetation of the two automatic landing systems (Section 4), the authors will use some information from [3], but will increase considerably the values of the sensor errors (biases) to study the robustness of the new ALS.

Putting together equations (5), (13), and (15), the following equation is obtained:

$$\begin{bmatrix} \dot{\boldsymbol{x}} \\ z_1 \\ z_2 \\ y \end{bmatrix} = \begin{bmatrix} A_{(8\times 8)} & B_{(8\times 2)} & G_{(8\times 3)} & 0_{(8\times 7)} \\ C_{0(1\times 8)} & D_{01(1\times 2)} & 0_{(1\times 3)} & 0_{(1\times 7)} \\ C_{1(1\times 8)} & D_{11(1\times 2)} & 0_{(1\times 3)} & 0_{(1\times 7)} \\ C_{(7\times 8)} & 0_{(7\times 2)} & 0_{(7\times 3)} & D_{22(7\times 7)} \end{bmatrix} \begin{bmatrix} \boldsymbol{x} \\ \boldsymbol{u} \\ \boldsymbol{u_w} \\ e \end{bmatrix}. \tag{16}$$

To proof that, in steady regime, the forms of $z_1 = \theta$ and $z_2 = u$ are the same with the ones in equation (13) and (16), we used the expansion of $z = \begin{bmatrix} z_1 & z_2 \end{bmatrix}^T$ as function of $\boldsymbol{x}$ and $\boldsymbol{u}$; for $\boldsymbol{u}_0$=0, we have successively obtained the following equations:

$$z = \begin{bmatrix} z_1 \\ z_2 \end{bmatrix} = z(\boldsymbol{x}, \boldsymbol{u}) \cong \underbrace{z(\boldsymbol{x}_0, \boldsymbol{u}_0)}_{z_0} + \left(\frac{\partial z}{\partial \boldsymbol{x}}\right)_{(\boldsymbol{x}_0, 0)} \Delta \boldsymbol{x} + \left(\frac{\partial z}{\partial \boldsymbol{u}}\right)_{(\boldsymbol{x}_0, 0)} \Delta \boldsymbol{u} \cong z_0 + \underbrace{\begin{bmatrix} \frac{\partial z_1}{\partial x_1} & \cdots & \frac{\partial z_1}{\partial x_n} \\ \frac{\partial z_2}{\partial x_1} & \cdots & \frac{\partial z_2}{\partial x_n} \end{bmatrix}_{(\boldsymbol{x}_0, 0)}}_{\begin{bmatrix} C_0 \\ C_1 \end{bmatrix}} \Delta \boldsymbol{x} + \underbrace{\begin{bmatrix} \frac{\partial z_1}{\partial u_1} & \frac{\partial z_1}{\partial u_2} \\ \frac{\partial z_2}{\partial u_1} & \frac{\partial z_2}{\partial u_2} \end{bmatrix}_{(\boldsymbol{x}_0, 0)}}_{\begin{bmatrix} D_{01} \\ D_{11} \end{bmatrix}} \Delta \boldsymbol{u} \Leftrightarrow \Delta z \cong \begin{bmatrix} C_0 \\ C_1 \end{bmatrix} \Delta \boldsymbol{x} +$$

$$+ \begin{bmatrix} D_{01} \\ D_{11} \end{bmatrix} \Delta \boldsymbol{u} \Leftrightarrow z \cong \begin{bmatrix} C_0 \\ C_1 \end{bmatrix} \boldsymbol{x} + \begin{bmatrix} D_{01} \\ D_{11} \end{bmatrix} \boldsymbol{u}, \quad \text{where} \quad C_0 = \begin{bmatrix} \frac{\partial z_1}{\partial x_1} & \cdots & \frac{\partial z_1}{\partial x_n} \end{bmatrix}_{(\boldsymbol{x}_0, 0)}, C_1 = \begin{bmatrix} \frac{\partial z_2}{\partial x_1} & \cdots & \frac{\partial z_2}{\partial x_n} \end{bmatrix}_{(\boldsymbol{x}_0, 0)}, \; x_i \left(i = \overline{1,8}\right) \text{ are the system's states,}$$

$u_i \left(i = \overline{1,2}\right)$ are the system's inputs $\left(\delta_{ec}, \delta_{Tc}\right)$, $D_{01} = \begin{bmatrix} \frac{\partial z_1}{\partial u_1} & \frac{\partial z_1}{\partial u_2} \end{bmatrix}_{(\boldsymbol{x}_0, 0)} = \begin{bmatrix} \frac{\partial \theta}{\partial \delta_{e_c}} & \frac{\partial \theta}{\partial \delta_{T_c}} \end{bmatrix}_{(\boldsymbol{x}_0, 0)} = \begin{bmatrix} c_1 & 0 \end{bmatrix}, D_{11} = \begin{bmatrix} \frac{\partial z_2}{\partial u_1} & \frac{\partial z_2}{\partial u_2} \end{bmatrix}_{(\boldsymbol{x}_0, 0)} =$

$$= \begin{bmatrix} \frac{\partial u}{\partial \delta_{e_c}} & \frac{\partial u}{\partial \delta_{T_c}} \end{bmatrix}_{(\boldsymbol{x}_0, 0)} = \begin{bmatrix} 0 & c_2 \end{bmatrix}. \quad \blacksquare$$

The control law $\boldsymbol{u}$ is calculated by using the formula: $\boldsymbol{u} = \hat{\boldsymbol{u}} + \bar{\boldsymbol{u}}$, where its first component $\left(\hat{\boldsymbol{u}}\right)$ is the optimal command calculated by means of the H_2/H_∞ method, while $\bar{\boldsymbol{u}}$ is determined by using the dynamic inversion. For obtaining $\hat{\boldsymbol{u}}$ (the output of the H_2/H_∞ controller), one has to minimize two cost functions. The first one, associated to the H_2 approach, is: $J_1 = \frac{1}{2} \int_0^\infty z_1^T z_1 \mathrm{d}t =$

$= \frac{1}{2} \int_0^\infty \left[\boldsymbol{x}^T \underbrace{\left(C_0^T C_0\right)}_{Q_0} \boldsymbol{x} + \hat{\boldsymbol{u}}^T \underbrace{\left(D_{01}^T D_{01}\right)}_{R_0} \hat{\boldsymbol{u}} \right] \mathrm{d}t$. In the case of H_2 approach, the optimal control law has been determined in [20] as:

$\hat{\boldsymbol{u}} = -K\hat{\boldsymbol{x}}, K = R_0^+ B^T P, R_0 = D_{01}^T D_{01}$; here, R_0^+ denotes the pseudo-inverse of the matrix R_0, the symmetric and positive defined matrix $P \in R^{8\times 8}$ is the stabilizing solution of the matrix Riccati equation [9]:

$$A^T P + PA - PBR_0^+ B^T P + Q_0 = 0, \tag{17}$$

while $\hat{\boldsymbol{x}}$ is the aircraft estimated state (obtained by means of an observer which will be designed by using the H_2 approach); denoting with $\Delta \boldsymbol{x}$ - the difference (deviation) between the aircraft real state ($\boldsymbol{x}$) state and its desired value $\left(\bar{\boldsymbol{x}}\right)$, i.e. $\Delta \boldsymbol{x} = \boldsymbol{x} - \bar{\boldsymbol{x}}$, by means of the observer borrowed from [20], i.e.:

$$\Delta \dot{\hat{\boldsymbol{x}}} = A\Delta \hat{\boldsymbol{x}} + B\boldsymbol{u} + G\boldsymbol{u_w} + L\left(\Delta y - C\Delta \hat{\boldsymbol{x}}\right), \tag{18}$$

we obtain the estimation of the signal $\Delta \boldsymbol{x}$, i.e. $\Delta \hat{\boldsymbol{x}} = \hat{\boldsymbol{x}} - \bar{\boldsymbol{x}}$; the observer gain matrix L is calculated as: $L = P^* C^T \left(D_{22}^T D_{22}\right)^{-1}$, with P^* – the stabilizing solution of the matrix Riccati equation [9]:

$$AP^* + P^* A^T - P^* C^T C P^* + GG^T = 0; \tag{19}$$

to design the observer (18), the vector of disturbances $\boldsymbol{u_w}$ has been estimated by the equipment from aircraft's navigation system.

The H_∞ control method combines the classical shaping and the notion of bandwidth with modern H_∞ robust stabilization; by using now this control approach, the system state equation, the equation of the output variable z_2, and the equation of the system measurement equation, one calculates, for the two landing stages, the optimal control law $\hat{\boldsymbol{u}}$ which minimizes the cost

function: $J_2 = \frac{1}{2}\int_0^\infty z_2^T z_2 \mathrm{d}t = \frac{1}{2}\int_0^\infty \left[\boldsymbol{x}^T \underbrace{\left(C_1^T C_1\right)}_{Q_1} \boldsymbol{x} + \hat{\boldsymbol{u}}^T \underbrace{\left(D_{11}^T D_{11}\right)}_{R_1} \hat{\boldsymbol{u}} \right] \mathrm{d}t$. As in the previous case (H_2 approach), the form of the optimal control law has been also deduced in [20]: $\hat{\boldsymbol{u}} = -K_\infty \hat{\boldsymbol{x}}, K_\infty = R_1^+ B^T P_\infty, R_1 = D_{11}^T D_{11}$; R_1^+ denotes the pseudo-inverse of the matrix R_1, while the symmetric and positive defined matrix $P_\infty \in R^{8\times 8}$ is the solution of the matrix Riccati equation [9], [20]:

$$A^T P_\infty + P_\infty A - P_\infty \left(B R_1^+ B^T - \mu_1^{-2} G G^T\right) P_\infty + Q_1 = 0. \tag{20}$$

Here, Q_1 and R_1 are positive matrices, while μ_1 is a small enough positive scalar for which the Riccati equation (20) has a stabilizing solution. The observer equation is again (18) with the gain matrix having the form: $L = L_\infty = P_\infty^* C^T \left(D_{22}^T D_{22}\right)^{-1} \in R^{8\times 7}$, where $P_\infty^* \in R^{8\times 8}$ is the stabilizing solution of the matrix Riccati equation:

$$A P_\infty^* + P_\infty^* A^T - P_\infty^* \left(C^T C - \mu_2^{-2} C_1^T C_1\right) P_\infty^* + G G^T = 0; \tag{21}$$

μ_2 has the same significance in (21) as μ_1 in (20), but these two constants can have the same values in some particular cases [9].

In order to obtain an optimum for the control law calculated both with H_2 and H_∞ approaches, i.e. to obtain the expression of the H_2/H_∞ control law, the following algorithm can be used:

Optimal algorithm [9]:

Step 1: The determination of the norms H_2 and H_∞ associated to the solutions of the Riccati equations (17), (19), (20), and (21);

Step 2: The calculation of the matrices $\hat{P} = (1-k)P + kP_\infty$, $\hat{P}^* = (1-k)P^* + kP_\infty^*$, with $k \in (0,1)$; in the numerical example (Section 5) we will choose k=0.5 but we will also analyze the effect of this constant's modification on the main variables' deviation with respect to their nominal value;

Step 3: The check of the following conditions' fulfillment: $\hat{P}, \hat{P}^* \geq 0, \hat{P}\hat{P}^* < I$.

Step 4: If the above conditions are not met, one chooses again the constant k and the steps 2 and 3 are again run;

Step 5: The final expression of the H_2/H_∞ control law is obtained with the equation: $\hat{\boldsymbol{u}} = -\hat{K}\hat{\boldsymbol{x}}, \hat{K} = R_1^+ B^T \hat{P}$, while the final expression of the observer gain matrix is $\hat{L} = \hat{P}^* C^T \left(D_{22}^T D_{22}\right)^{-1}$. ■

3.2. Design of the second component (guidance component - $\bar{\boldsymbol{u}}$) of the control law $\boldsymbol{u}$

We consider the vector $\bar{z} = \left[\bar{\theta} \quad \bar{u}\right]^T$ containing the reference variables (the desired values of the pitch angle and longitudinal velocity, respectively). By using $\bar{z}$ and the dynamic inversion principle, we calculate $\bar{\boldsymbol{x}}$ (the desired state of the system) and $\bar{\boldsymbol{u}}$ (the desired control) with respect to $\bar{z}$ and, after that, the vector $\bar{y}$ is obtained with the equations: $\dot{\bar{\boldsymbol{x}}} = A\bar{\boldsymbol{x}} + B\bar{\boldsymbol{u}}$, $\bar{z} = C'\bar{\boldsymbol{x}}, \bar{y} = C\bar{\boldsymbol{x}}; C' = \begin{bmatrix} C_0 \\ C_1 \end{bmatrix}$, with C_0 and C_1 having the forms (14). Now, a coordinates' change is achieved by means of the transformation matrix $T \in R^{8\times 8}$ [6]:

$$\begin{bmatrix} \xi \\ \eta \end{bmatrix} = T\boldsymbol{x}, \boldsymbol{x} = T^{-1}\begin{bmatrix} \xi \\ \eta \end{bmatrix}, \xi = \left[z_1 \quad \dot{z}_1 \quad \cdots \quad z_1^{(\eta_1-1)} \quad z_2 \quad \dot{z}_2 \quad \cdots \quad z_2^{(r_2-1)} \quad \cdots \quad z_p \quad \dot{z}_p \quad \cdots \quad z_p^{(r_p-1)}\right]^T; \tag{22}$$

ξ is a state vector consisting of the controlled variables and their derivates, with $z_i^{(r_i-1)}$ – the (r_i-1) order derivative of z_i; for the aircraft dynamics in longitudinal plane, $z_1=\theta$, $z_2=z_p=u$. The second state vector (η) contains the states which are not included in the vector ξ; the dimension of vector η is $n - r = n - \sum_{i=1}^{p} r_i$, where n is the dimension of the square matrix T, while the values of r_i are deduced below. Thus, one derivates with respect to time the equations of z_1 and z_2 until the terms containing the components of the control law $(\delta_{ec}, \delta_{Tc})$ appear; one yields:

$$\begin{aligned}
\dddot{\theta} &= a'_{41}\frac{u}{V_0} + a'_{42}\alpha + a'_{43}q + a'_{44}\theta + a'_{47}\delta_e + a'_{48}\delta_T + \frac{b_{31}}{T_e}\delta_{ec} + \frac{b_{32}}{T_T}\delta_{Tc} + a'_{41}\frac{u_g}{V_0} + a'_{42}\alpha_g + a'_{43}q_g + V_0 a_{31}\frac{\dot{u}_g}{V_0} + V_0 a_{33}\dot{\alpha}_g + a_{33}\dot{q}_g, \\
\ddot{u} &= a'_{11}\frac{u}{V_0} + a'_{12}\alpha + a'_{13}q + a'_{14}\theta + a'_{17}\delta_e + a'_{18}\delta_T + \frac{b_{11}}{T_e}\delta_{ec} + \frac{b_{12}}{T_T}\delta_{Tc} + g'_{11}\frac{u_g}{V_0} + g'_{12}\alpha_g + g'_{13}q_g + g_{11}\frac{\dot{u}_g}{V_0} + g_{12}\dot{\alpha}_g,
\end{aligned} \tag{23}$$

with

$$a'_{41}=V_0\left(a_{11}a_{31}+a_{21}a_{33}+a_{31}a_{33}\right), a'_{42}=V_0\left(a_{12}a_{31}+a_{22}a_{33}+a_{31}a_{33}\right), a'_{43}=a_{23}a_{33}+a_{33}^2+a_{34},$$
$$a'_{44}=a_{31}a_{14}, a'_{47}=a_{31}b_{11}+a_{32}b_{21}+a_{33}b_{31}-\frac{b_{31}}{T_e}, a'_{48}=a_{31}b_{12}+a_{33}b_{22}+a_{33}b_{32}-\frac{b_{32}}{T_T};$$
$$a'_{11}=V_0\left(a_{11}^2+a_{12}a_{21}\right), a'_{12}=V_0\left(a_{11}a_{12}+a_{12}a_{22}\right), a'_{13}=a_{12}a_{23}+a_{14}, a'_{14}=a_{11}a_{14}, a'_{17}=a_{11}b_{11}+a_{12}b_{21}-\frac{b_{11}}{T_e},$$
$$a'_{18}=a_{11}b_{12}+a_{12}b_{21}-\frac{b_{12}}{T_T}, g'_{11}=V_0\left(a_{11}^2+a_{12}a_{21}\right), g'_{12}=V_0\left(a_{11}a_{12}+a_{12}a_{22}\right), g'_{13}=a_{14}, g_{11}=V_0a_{11}, g_{12}=V_0a_{12}. \quad (24)$$

According to (23), the relative degrees are r_1=3 and r_2=2 and the equations (23) may be combined into a single one: $z^{(r)}=A_x\boldsymbol{x}+B_u\bar{\boldsymbol{u}}+G'\boldsymbol{u}_w+G''\dot{\boldsymbol{u}}_w$, with $z^{(r)}=\left[z_1^{(r_1)}\quad z_2^{(r_2)}\right]^T=\left[\ddot{\theta}\quad\ddot{u}\right]^T, \bar{\boldsymbol{u}}=\left[\delta_{ec}\quad\delta_{Tc}\right]^T, A_x=\begin{bmatrix}a'_{41}&a'_{42}&a'_{43}&a'_{44}&0&0&a'_{47}&a'_{48}\\ a'_{11}&a'_{12}&a'_{13}&a'_{14}&0&0&a'_{17}&a'_{18}\end{bmatrix}$,

$$B_u=\begin{bmatrix}\frac{b_{31}}{T_e}&\frac{b_{32}}{T_T}\\ \frac{b_{11}}{T_e}&\frac{b_{12}}{T_T}\end{bmatrix}, G'=\begin{bmatrix}a'_{41}&a'_{42}&a'_{43}\\ g'_{11}&g'_{12}&g'_{13}\end{bmatrix}, G''=\begin{bmatrix}V_0a_{31}&V_0a_{33}&a_{33}\\ g_{11}&g_{12}&0\end{bmatrix}.$$

For the glide slope phase, the state vectors ξ and η are: $\xi=\left[\theta\quad\dot{\theta}\quad\ddot{\theta}\quad u\quad\dot{u}\right]^T, \eta=\left[\frac{H}{V_0}\quad\frac{\dot{H}}{V_0}\quad\delta_e\right]^T$, while, for the second phase of landing, these vectors are, respectively: $\xi=\left[\theta\quad\dot{\theta}\quad\ddot{\theta}\quad u\quad\dot{u}\right]^T, \eta=\left[\frac{H}{V_0}\quad\frac{\tilde{H}_c}{V_0}\quad\delta_e\right]^T$.

Using the coordinates' change (22) [6], considering $\boldsymbol{u}_w=0$ and $\boldsymbol{u}=\bar{\boldsymbol{u}}$, the system (5) gets the form: $\begin{bmatrix}\dot{\xi}\\ \dot{\eta}\end{bmatrix}=\hat{A}\begin{bmatrix}\xi\\ \eta\end{bmatrix}+\hat{B}\bar{\boldsymbol{u}}$; $\hat{A}=TAT^{-1}, \hat{B}=TB$. If the matrices $\hat{A}$ and $\hat{B}$ are partitioned with respect to the dimensions of vectors ξ and η, it results [6]:

$$\begin{bmatrix}\dot{\xi}\\ \dot{\eta}\end{bmatrix}=\begin{bmatrix}\hat{A}_{11}&\hat{A}_{12}\\ \hat{A}_{21}&\hat{A}_{22}\end{bmatrix}\begin{bmatrix}\xi\\ \eta\end{bmatrix}+\begin{bmatrix}\hat{B}_1\\ \hat{B}_2\end{bmatrix}\bar{\boldsymbol{u}}; \quad (25)$$

the matrices in the above equation have the following dimensions: $\hat{A}_{11}\in R^{5\times5}, \hat{A}_{12}\in R^{5\times3}, \hat{A}_{21}\in R^{3\times5}, \hat{A}_{22}\in R^{3\times3}, \hat{B}_1\in R^{5\times2}, \hat{B}_2\in R^{3\times2}$. The matrix A has the form (10) for the glide slope phase and the form (12) for the second landing phase; as a consequence, the matrices $\hat{A}$ and $\hat{A}_{ij}, i,j=\overline{1,2}$, modify during the transition from the first landing phase to the second one.

Equation (25) is equivalent with:

$$\dot{\xi}=\hat{A}_{11}\xi+\hat{A}_{12}\eta+\hat{B}_1\bar{\boldsymbol{u}}, \dot{\eta}=\hat{A}_{21}\xi+\hat{A}_{22}\eta+\hat{B}_2\bar{\boldsymbol{u}}. \quad (26)$$

Imposing $\xi=\bar{\xi}$ and $\dot{\xi}=\dot{\bar{\xi}}$, with $\bar{\xi}=\left[\bar{\theta}\quad\bar{\dot{\theta}}\quad\bar{\ddot{\theta}}\quad\bar{u}\quad\bar{\dot{u}}\right]^T, \dot{\bar{\xi}}=\left[\bar{\dot{\theta}}\quad\bar{\ddot{\theta}}\quad\bar{\dddot{\theta}}\quad\bar{\dot{u}}\quad\bar{\ddot{u}}\right]^T$, from equation (26) the command vector $\bar{\boldsymbol{u}}$ is obtained as follows:

$$\bar{\boldsymbol{u}}=\hat{B}_1^{+}\left(\dot{\bar{\xi}}-\hat{A}_{11}\bar{\xi}-\hat{A}_{12}\eta\right). \quad (27)$$

In order to obtain the matrix T, the vectors ξ and η are replaced in (22); for the glide slope, one obtains:

$$\begin{bmatrix}\theta\\ \dot{\theta}\\ \ddot{\theta}\\ u\\ \dot{u}\\ \frac{H}{V_0}\\ \frac{\dot{H}}{V_0}\\ \delta_e\end{bmatrix}=\underbrace{\begin{bmatrix}0&0&0&1&0&0&0&0\\ 0&0&1&0&0&0&0&0\\ V_0a_{31}&V_0a_{32}&a_{33}&a_{34}&0&0&b_{31}&b_{32}\\ V_0&0&0&0&0&0&0&0\\ V_0a_{11}&V_0a_{12}&0&a_{14}&0&0&b_{11}&b_{12}\\ 0&0&0&0&1&0&0&0\\ 0&0&0&0&0&1&0&0\\ 0&0&0&0&0&0&1&0\end{bmatrix}}_{T}\begin{bmatrix}\frac{u}{V_0}\\ \alpha\\ q\\ \theta\\ \frac{H}{V_0}\\ \frac{\dot{H}}{V_0}\\ \delta_e\\ \delta_T\end{bmatrix}; \quad (28)$$

for the second landing phase, in (28) $\frac{\dot{H}}{V_0}$ is replaced by $\frac{\tilde{\dot{H}}_c}{V_0}$. Now, replacing $\bar{\xi}$ and $\dot{\bar{\xi}}$ in (27), one gets:

$$\bar{\boldsymbol{u}} = \hat{B}_1^+ \left\{ \begin{bmatrix} 0 \\ 0 \\ \dddot{\bar{\theta}} \\ 0 \\ \ddot{\bar{u}} \end{bmatrix} - \begin{bmatrix} \hat{a}_{11} & (\hat{a}_{12}-1) & \hat{a}_{13} & \hat{a}_{14} & \hat{a}_{15} \\ \hat{a}_{21} & \hat{a}_{22} & (\hat{a}_{23}-1) & \hat{a}_{24} & \hat{a}_{25} \\ \hat{a}_{31} & \hat{a}_{32} & \hat{a}_{33} & \hat{a}_{34} & \hat{a}_{35} \\ \hat{a}_{41} & \hat{a}_{42} & \hat{a}_{43} & \hat{a}_{44} & (\hat{a}_{45}-1) \\ \hat{a}_{51} & \hat{a}_{52} & \hat{a}_{53} & \hat{a}_{54} & \hat{a}_{55} \end{bmatrix} \bar{\xi} - \hat{A}_{12}\eta \right\} \tag{29}$$

or $\bar{\boldsymbol{u}} = \hat{B}_1^+ \left\{ \begin{bmatrix} 0 & 0 & \dddot{\bar{\theta}} & 0 & \ddot{\bar{u}} \end{bmatrix}^T - \hat{A}'_{11}\,\bar{\xi} - \hat{A}_{12}\eta \right\}$, where $\hat{A}'_{11}$ is calculated from $\hat{A}_{11}$ making the substitutions $\hat{a}'_{12} = \hat{a}_{12} - 1$, $\hat{a}'_{23} = \hat{a}_{23} - 1, \hat{a}'_{45} = \hat{a}_{45} - 1$, the other elements of the matrices $\hat{A}_{11}$ and $\hat{A}'_{11}$ being the same; $\hat{a}_{ij}$, i, $j = \overline{1,5}$ are the elements of the matrix $\hat{A}_{11}$.

Replacing (26) in (29), with $\xi = \bar{\xi}$, one successively obtains

$$\begin{aligned} \dot{\eta} &= \hat{A}_{21}\bar{\xi} + \hat{A}_{22}\eta + \hat{B}_2\hat{B}_1^+ \left\{ \begin{bmatrix} 0 & 0 & \dddot{\bar{\theta}} & 0 & \ddot{\bar{u}} \end{bmatrix}^T - \hat{A}'_{11}\,\bar{\xi} - \hat{A}_{12}\eta \right\} = \\ &= \left(\hat{A}_{22} - \hat{B}_2\hat{B}_1^+\hat{A}_{12}\right)\eta + \left(\hat{A}_{21} - \hat{B}_2\hat{B}_1^+\hat{A}'_{11}\right)\bar{\xi} + \hat{B}_2\hat{B}_1^+ \begin{bmatrix} 0 & 0 & \dddot{\bar{\theta}} & 0 & \ddot{\bar{u}} \end{bmatrix}^T; \end{aligned} \tag{30}$$

(30) can be expressed as:

$$\dot{\eta} = \hat{A}_\eta\,\eta + \hat{B}_z\bar{z}^{(r)} + \hat{A}_\xi\bar{\xi} \Leftrightarrow \dot{\eta} = \hat{A}_\eta\,\eta + \hat{B}_y\bar{Z}, \tag{31}$$

where

$$\begin{aligned} &\hat{A}_\eta = \hat{A}_{22} - \hat{B}_2\hat{B}_1^+\hat{A}_{12}, \hat{A}_\xi = \hat{A}_{21} - \hat{B}_2\hat{B}_1^+\hat{A}'_{11}, \hat{B}_z\bar{z}^{(r)} = \hat{B}_2\hat{B}_1^+ \begin{bmatrix} 0 & 0 & \dddot{\bar{\theta}} & 0 & \ddot{\bar{u}} \end{bmatrix}^T, \\ &\bar{z}^{(r)} = \begin{bmatrix} \bar{z}_1^{(r_1)} & \bar{z}_2^{(r_2)} \end{bmatrix}^T = \begin{bmatrix} \dddot{\bar{\theta}} & \ddot{\bar{u}} \end{bmatrix}^T, \hat{B}_y = \begin{bmatrix} \hat{B}_z & \hat{A}_\xi \end{bmatrix}, \bar{Z} = \begin{bmatrix} \bar{z}^{(r)} & \bar{\xi} \end{bmatrix}^T = \begin{bmatrix} \dddot{\bar{\theta}} & \ddot{\bar{u}} & \bar{\theta} & \dot{\bar{\theta}} & \ddot{\bar{\theta}} & \bar{u} & \dot{\bar{u}} \end{bmatrix}^T. \end{aligned} \tag{32}$$

The dimensions of the above matrices are: $\hat{A}_\eta \in R^{3\times3}, \hat{A}_\xi \in R^{3\times5}, \hat{B}_z \in R^{2\times2}, \hat{B}_y \in R^{3\times7}$. If $\hat{B}_2\hat{B}_1^+ = \begin{bmatrix} \hat{b}_{11} & \hat{b}_{12} & \hat{b}_{13} & \hat{b}_{14} & \hat{b}_{15} \\ \hat{b}_{21} & \hat{b}_{22} & \hat{b}_{23} & \hat{b}_{24} & \hat{b}_{25} \\ \hat{b}_{31} & \hat{b}_{32} & \hat{b}_{33} & \hat{b}_{34} & \hat{b}_{35} \end{bmatrix}$, then $\hat{B}_z^T = \begin{bmatrix} \hat{b}_{13} & \hat{b}_{23} & \hat{b}_{33} \\ \hat{b}_{15} & \hat{b}_{25} & \hat{b}_{35} \end{bmatrix}$. Thus, for the calculation of vector $\bar{\boldsymbol{u}}$, one solves equation (31) – second form and obtains the vector η and then uses equation (29). From the expression of $\hat{B}_z\bar{z}^{(r)}$ (equation (32)), it results: $\hat{B}_1^+ \begin{bmatrix} 0 & 0 & \dddot{\bar{\theta}} & 0 & \ddot{\bar{u}} \end{bmatrix}^T = \hat{B}_2^+\hat{B}_z\bar{z}^{(r)}$, which, replaced into (29), leads to the following one:

$$\bar{\boldsymbol{u}} = \hat{B}_u^{-1}\left(\bar{z}^{(r)} - \hat{B}_\xi\bar{\xi} - \hat{B}_\eta\eta\right), \tag{33}$$

with $\hat{B}_u^{-1} = \hat{B}_2^+\hat{B}_z, \hat{B}_\xi = \hat{B}_u\hat{B}_1^+\hat{A}'_{11}, \hat{B}_\eta = \hat{B}_u\hat{B}_1^+\hat{A}_{12}$; these matrices have the following dimensions: $\hat{B}_u \in R^{2\times2}, \hat{B}_\xi \in R^{2\times5}, \hat{B}_\eta \in R^{2\times3}$. Therefore, $\bar{\boldsymbol{u}}$ can be obtained by means of equation (29) or by using equation (33).

Another form of the command law $\bar{\boldsymbol{u}}$ results from the equation $z^{(r)} = A_x\boldsymbol{x} + B_u\bar{\boldsymbol{u}} + G'\boldsymbol{u}_w + G''\dot{\boldsymbol{u}}_w$, if we impose the convergence of $z^{(r)} = \begin{bmatrix} \ddot{\theta} & \dot{u} \end{bmatrix}^T$ to $\bar{z}^{(r)} = \begin{bmatrix} \dddot{\bar{\theta}} & \ddot{\bar{u}} \end{bmatrix}^T$ and the convergence of the system estimated state $(\hat{\boldsymbol{x}})$ to $\boldsymbol{x}$; in these conditions, it yields:

$$\bar{\boldsymbol{u}} = \hat{B}_u^{-1}\left(\bar{z}^{(r)} - A_x\hat{\boldsymbol{x}} - G'\boldsymbol{u}_w - G''\dot{\boldsymbol{u}}_w\right), \tag{34}$$

with $\hat{B}_u, A_x, G'$ and G'' having the same forms as above.

3.3. The structure of the new automatic landing system

The structure of the new automatic landing system using the H_2/H_∞ control technique, the dynamic inversion method, two reference models, an optimal observer, and the geometry of landing is presented in fig. 1. Here, the variables with a line above mean the desired (commanded) values of these variables, while the matrix C_r has the form $C_r = \begin{bmatrix} 0 & 0 & 0 & 0 & 1 & 0 & 0 \end{bmatrix}$.

Taking into account all the above equations, it can be concluded that the automatic control of the aircraft in longitudinal plane, during landing, is mainly based on the dynamic inversion and H_2/H_∞ method. The vector $\bar{Z}$ may be calculated by means of two reference models, the former being a third order reference model, while the latter is a second order reference model (fig. 2) [7]. On the other hand, aircraft landing is simplified if its motion in lateral plane is made without errors (deviation of the aircraft from the runway direction is zero). Therefore, before the start of the glide slope and flare phases, the pilot must cancel the aircraft lateral deviation with respect to the runway; this can be achieved by means of different control systems for the flight direction control [11, 13, 21].

The obtaining of the aircraft desired landing trajectory mainly involves two variables' control: the pitch angle (θ) and the forward speed (*u*). According to the landing requirements for Boeing 747, the aircraft must descend from cruising altitude to a lower altitude around 420 m. Meanwhile, the aircraft speed is also reduced from the cruising speed to an approach value and, after that, it remains constant. So, when we design the desired trajectory, we design the desired forward speed *u* first of all. The optimal control system associated to aircraft flight during landing (longitudinal plane), based on H_2/H_∞ and dynamic inversion techniques, and the optimal observer must assure the convergences: $\Delta y = y - \bar{y} \to 0 \left(y = C\boldsymbol{x} \to \bar{y} = C\bar{\boldsymbol{x}}, \boldsymbol{x} \to \bar{\boldsymbol{x}}\right), \Delta \boldsymbol{x} = \boldsymbol{x} - \bar{\boldsymbol{x}} \to 0$ $\left(\hat{\boldsymbol{x}} \to \boldsymbol{x} \to \bar{\boldsymbol{x}}\right)$; here, $\bar{\boldsymbol{x}}$ is the aircraft desired state, while $\bar{y}$ is the reference vector associated to the measured output *y*.

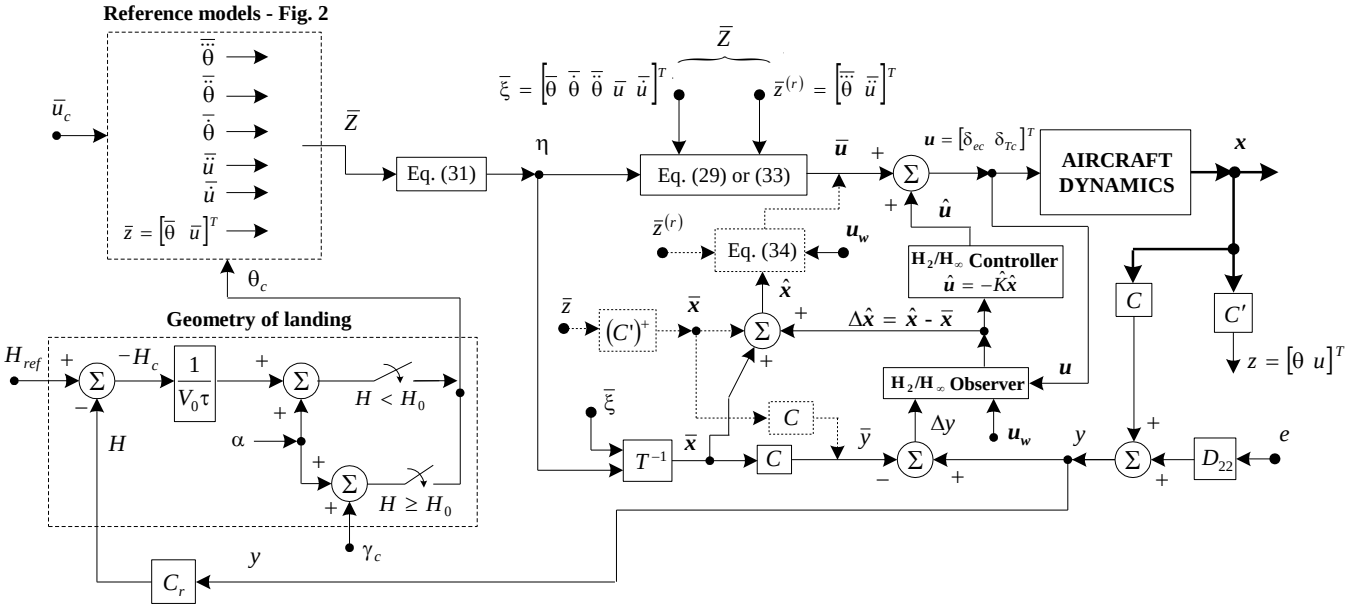

Fig. 1 Automatic landing system for aircraft control in longitudinal plane using the H_2/H_∞ control and the dynamic inversion

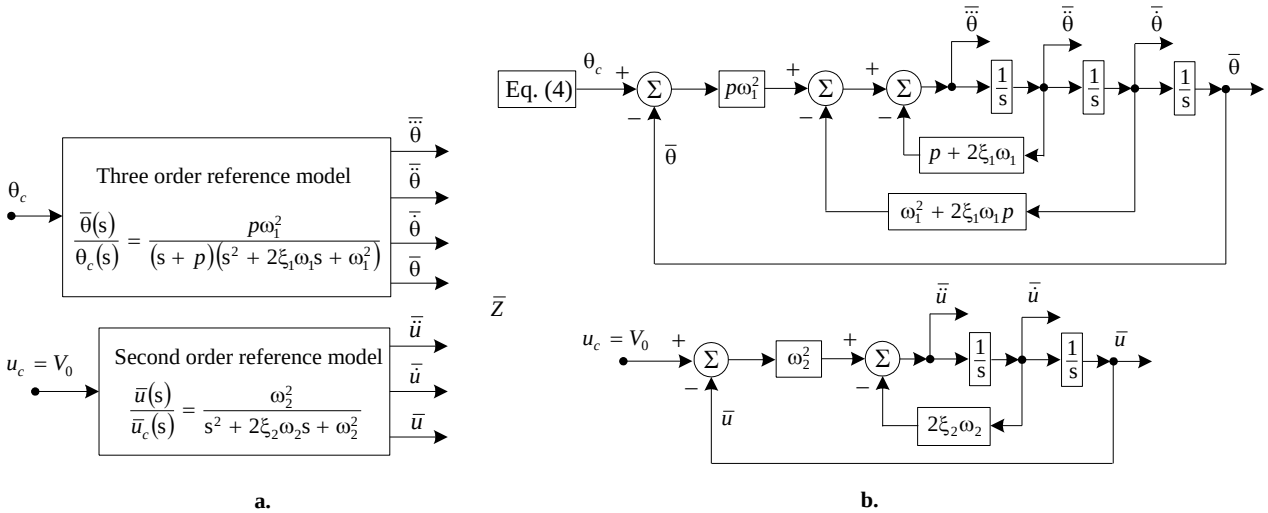

a. **b.**

Fig. 2 Block diagrams of the three order and second order reference models, respectively: a) simplified block diagrams; b) detailed block diagrams

4. Numerical Simulation Results

4.1. Numerical simulation setup

To study the performances of the new obtained automatic landing system, one considers the landing of a Boeing 747. Complex simulations in Matlab/Simulink environment have been performed; thus, one designed the optimal observer, the H_2/H_∞ controller, the component obtained with the dynamic inversion method, and, after that, validated the proposed automatic landing system. The values of the coefficients for Boeing 747 dynamics have been borrowed from [6]: $a_{11} = -0.021, a_{12} = 0.122, a_{14} = -0.322, a_{21} = -0.209, a_{22} = -0.53, a_{23} = 2.21, a_{24} = 0, a_{31} = 0.017, a_{32} = -0.164, a_{33} = -0.412,$ $a_{34} = 0, b_{11} = 0.01, b_{12} = 1, b_{21} = -0.064, b_{22} = -0.044, b_{31} = -0.378, b_{32} = 0.544, u_c = \bar{u}_c = \bar{u} = V_0 = 70\,\text{m/s}, T_e = T_T = 0.9\,\text{s},$ $\tau = 4, c_1 = 0.31, c_2 = 3.16, \mu_1 = 50, \mu_2 = 100$. Because the H_2/H_∞ technique deals with linearized dynamics, use used here the linear dynamics of aircraft (equation (5)). The advantage of this technique is that it handles the plants having sensor errors and other disturbances – a real problem during aircraft landing. We neglected the time-delays and we considered the biases of the sensors – the only sensor errors (the measurement noises have been not taken into account). The elements of matrix *G* have been calculated with (11); for the two stages of landing, the vector containing the sensor errors (biases associated to the measurement process) is $e = [0.1\,\text{m/s} \quad 0.1\,\text{deg} \quad 0\,\text{deg/s} \quad 0.1\,\text{deg} \quad 0\,\text{m} \quad 0.1\,\text{deg} \quad 0.1\,\text{deg}]^T$, while, for the reference models, one has chosen: $p = 25, \xi_1 = \ = \xi_2 = 0.7, \omega_1 = \omega_2 = 2\,\text{rad/s}$. The values considered in this paper for the sensor errors are chosen very large because it is important to use strong disturbances instead of small ones when designing a robust ALS. For the landing two phases, the following initial states were considered: $\boldsymbol{x}(0) = [1.0143 \quad -0.5\,\text{deg} \quad 2\,\text{deg/ s} \quad -2.5\,\text{deg} \quad 6\,\text{s} \quad 0 \quad -3\,\text{deg} \quad 2\,\text{deg}]^T$ and $\boldsymbol{x}(0) = [1 \quad -0.1\,\text{deg} \quad 0\,\text{deg/ s} \quad -2.5\,\text{deg} \quad 0.428\,\text{s} \quad 0 \quad -2\,\text{deg} \quad 0\,\text{deg}]^T$, respectively. The disturbances, additionally introduced in the state equations, are $\boldsymbol{u}_w = [-1.057 \quad 0.05 \quad 0\,\text{deg/ s}]^T$ – first landing phase, and $\boldsymbol{u}_w = [-1.13 \quad 0.05 \quad 0\,\text{deg/ s}]^T$ – second landing phase, respectively.

4.2. Results and discussion

In figs. 3 and 4 we represent the time characteristics for the glide slope phase and flare phase, respectively; the characteristics have been represented for the new ALS affected by disturbances in the presence or in the absence of sensor errors (the sensors are used for the measurement of the states). The last three mini-graphics in these two figures represent the deviations of the forward speed (*u*), slope angle (γ), and altitude (*H*), with respect to their nominal values, i.e. $\bar{u} - u, \gamma_c - \gamma, H_{ref} - H$. The presence of the sensor errors is not visible: the curves with solid line (obtained for the ALS without sensor errors) overlap almost perfectly over the curves plotted with dashed line (obtained for the ALS with sensor errors). The time origin for the flare trajectory is chosen zero when the altitude is $H=H_0$=30 m (the altitude at which the glide slope phase ends).

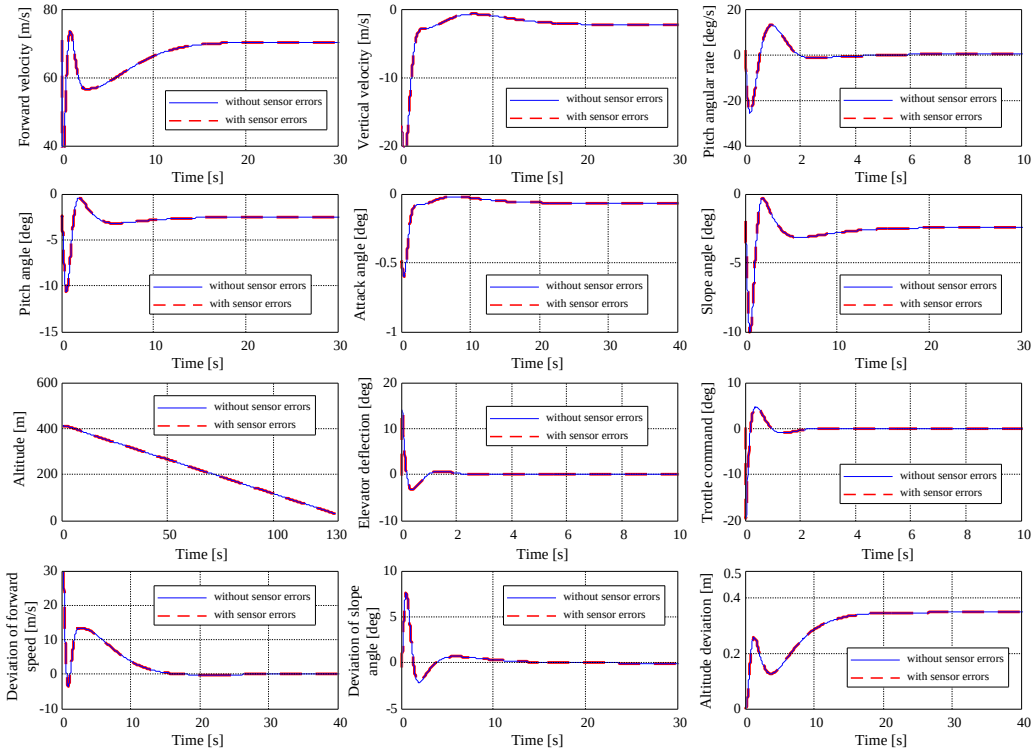

Fig. 3 Time characteristics for the glide slope phase, with or without sensor errors

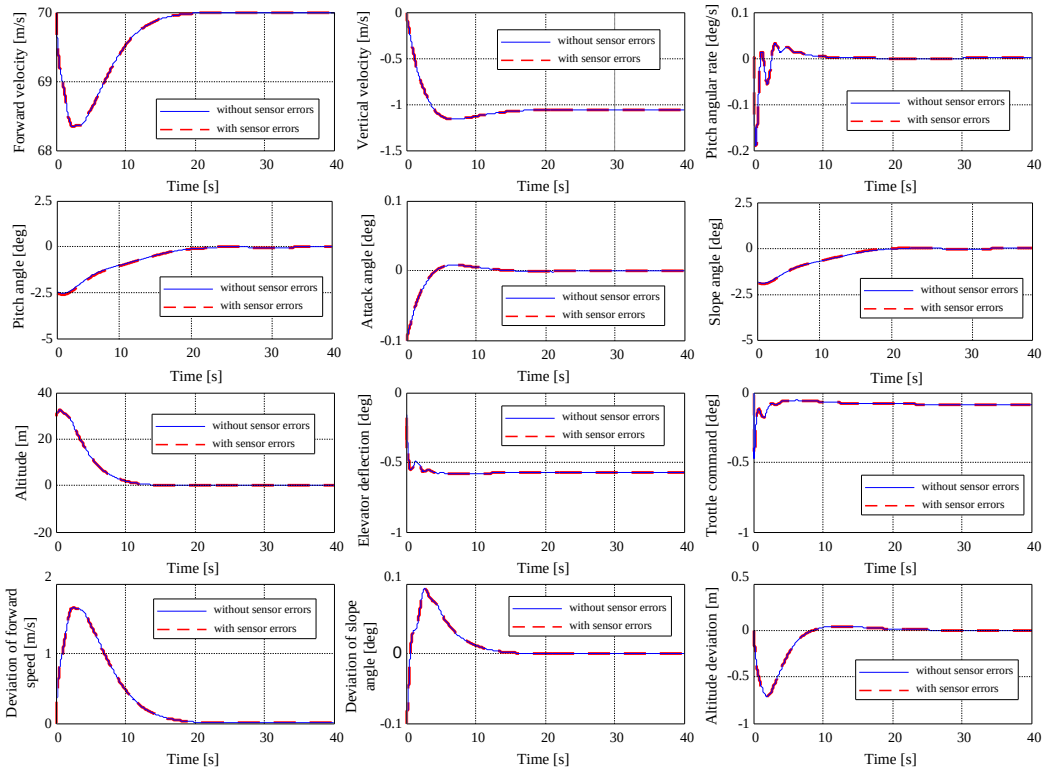

Fig. 4 Time characteristics for the flare phase, with or without sensor errors

From the theoretical part of this paper, we retained the mandatory values of the slope angle (the difference between the pitch angle and the attack angle): -2.5 degrees in the first landing phase and 0 degrees in the second phase, respectively. By analyzing figs. 3 and 4, we remark the correctness of the simulation data. During the glide slope, the aircraft must have a linear descendent trajectory (fig. 3.g) and, as a consequence, the pitch angle must be negative; as one can see in fig. 3, the pitch angle is -2.53 degrees, while the attack angle is slightly negative $(\cong -0.03\text{deg})$; it results the desired slope angle (-2.5 degrees). In the flare phase, the aircraft must describe a parabolic trajectory (fig. 4.g) with a null slope angle; as one can see in fig. 4, the pitch and the attack angles become zero in about 14 seconds; it results the desired null slope angle.

The landing begins at a longitudinal speed initially exceeding the nominal speed by 1 m/s (see fig. 3.a). The speed should be reduced to the normal speed (70 m/s) and then kept at this value; this landing process begins at 420 m (fig. 3.g). To test the robustness of the new ALS, in all simulations, we have taken into consideration the disturbances. From last graphic in figs. 3 and 4, we can see that the final error between the desired path and the actual path is less than 0.35 m during the glide slope phase and very close to 0 m for flare. These errors are very small if the Federal Aviation Administration (FAA) accuracy requirements for Category III (the best category) [22] are analyzed; according to FAA Category III accuracy requirements, the vertical error (altitude deviation with respect to its nominal value) must be less than 0.5 m, the lateral deviation must be less than 4.1 m, while the final altitude at the end of flare must be 0 m. The robustness of our new automatic landing system is due to the H_2/H_∞ control technique, this method being capable to handle the plant with sensor errors and disturbances. From the forward speed point of view, the error is less than 0.01m/s (fig. 3.j and fig. 4.j); because the deviation of the slope angle with respect to its nominal value $(\gamma_c - \gamma)$ tends to zero we conclude that $\gamma \to \gamma_c = -2.5\text{deg}$, for the first landing phase, and $\gamma \to \gamma_c = 0\text{deg}$ for the second landing phase. The optimal control system associated to aircraft flight during landing, based on H_2/H_∞ technique, assures the convergence $H \to H_{ref}$, for both cases when the sensor errors are taken or not into account.

For Boeing 747 (the aircraft chosen in this paper for the validation of our new ALS), the first phase of the landing process takes approximately 129 seconds (fig. 3.g), while the second phase of the landing (flare phase) takes approximately 25 seconds (fig. 4.g); in the same time, the steady values of aircraft vertical velocity are $w \cong -2.2\,\text{m/s}$ (glide slope – fig. 3) and $w \cong -1.06\,\text{m/s}$ (flare – fig. 4), respectively. During the two stages of landing, the vertical velocity mean values are $w_{mean} \cong -3.02\,\text{m/s}$ and $w_{mean} \cong -1.2\,\text{m/s}$, respectively. Using this information, the vertical distance covered by the aircraft in the first landing phase must be approximately $3.02\,\text{m/s} \cdot 129\,\text{s} = 389.58\,\text{m}$, while the vertical distance covered in the second landing phase must be approximately $1.2\,\text{m/s} \cdot 25\,\text{s} = 30\,\text{m}$. These values are again confirmed by figs. 3 and 4 since the glide slope phase means a 390 m descent for the aircraft center of gravity, while the flare phase means a 30 m descend.

In Section 3.1, the matrix D_{22} (the matrix of weights associated to the sensor errors) has been chosen as $D_{22} = \bar{k} I_7$ ($\bar{k}$ – positive constant, $\bar{k} = \det(D_{22})$); for figs. 3 and 4, we have used the value $\bar{k} = 1$, but it is interesting to see what happens if this constant is increased. According to the expressions of the observer gain matrices L and L_∞, a change of the matrix D_{22} is

equivalent with a modification of these two matrices and, according to the equation $\hat{L} = \hat{P}^* C^T \left(D_{22}^T D_{22}\right)^{-1}$, this change also means a modification of the observer final gain matrix $\left(\hat{L}\right)$, of the observer errors, and of all the variables' time history. In figs. 5 and 6 we represent, beside the aircraft altitude, the time histories associated to the deviations of the altitude, forward speed, and slope angle, with respect to their nominal values, i.e. $H_{ref} - H, \bar{u} - u, \gamma_c - \gamma$ for different values of the matrix D_{22}; we have chosen 5 values for the constant $\bar{k}$, i.e.: 1, 1.1, 1.3, 1.4, and 1.6.

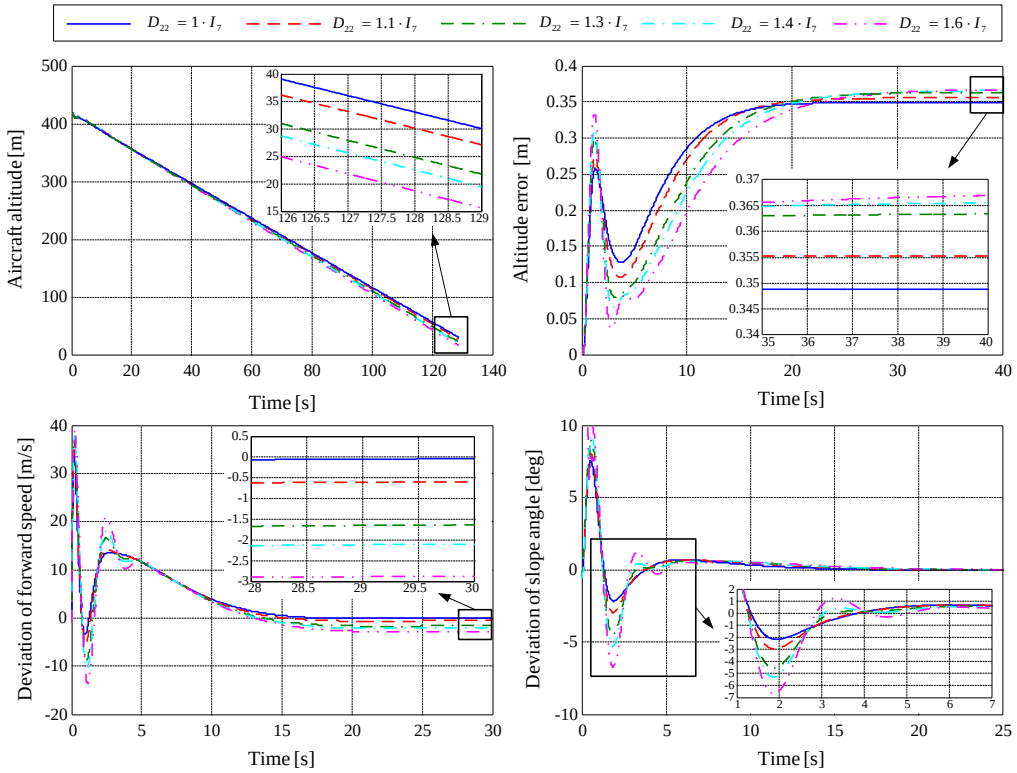

Fig. 5 Aircraft altitude and the main errors during glide slope for different matrix D_{22}

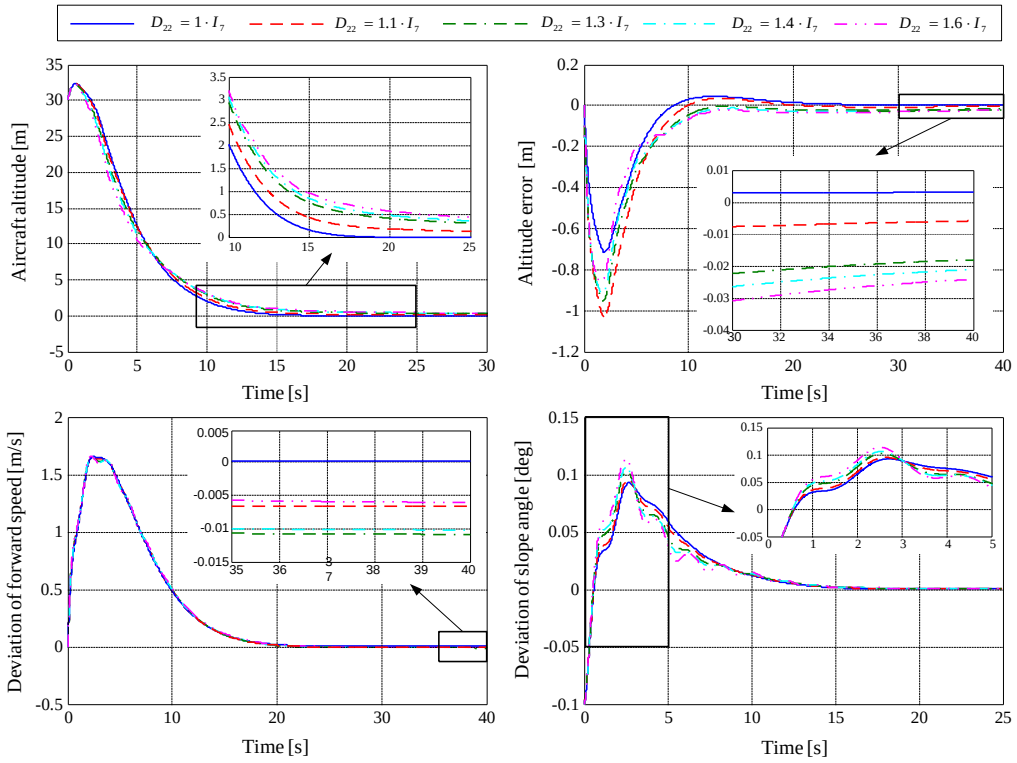

Fig. 6 Aircraft altitude and the main errors during flare for different matrix D_{22}

For the first landing phase, as one can see in fig. 5.a, the altitude decays faster for bigger values of the constant $\bar{k}$; this means that an increase of $\bar{k}$ is equivalent with the decrease of the glide slope duration and horizontal distance covered during this first stage of landing: the glide slope duration is 129 seconds for $\bar{k}=1$, 128 seconds for $\bar{k}=1.1$, 126.3 seconds for $\bar{k}=1.3$, 125.5 seconds for $\bar{k}=1.4$, and 124.4 seconds for $\bar{k}=1.6$ (fig. 5.a). This is because the aircraft speed increases together with the constant $\bar{k}$ (fig. 5.c); a bigger speed, for a constant slope (fig. 5.d), means a more rapid linear descend, but the negative effect is that the error $\bar{u}-u$ has increased from zero $(\bar{k}=1)$ to -2.78 m/s $(\bar{k}=1.6)$. Because H_{ref} is constant, the increase of the constant $\bar{k}$ is also equivalent with the increase of the aircraft altitude error (fig. 5.b); this altitude error slightly increases together with the constant $\bar{k}$ from 0.35 to 0.365. On the other hand, the variation of $\bar{k}$ does not modify the glide slope angle (fig. 5.d), but it increases the overshoots and the transient regimes.

For the flare stage, as one can see in the fig. 6.a, the influence of D_{22}'s modification is different especially from the speed and flare duration point of view; thus, the increase of the constant $\bar{k}$ means: 1) the increase of the altitude stationary value from a value very close to 0 m to 0.25 m (figs. 6.a and 6.b); 2) the increase of the altitude error absolute value $\left|H_{ref}-H\right|$ from a value very close to 0 m to 0.25 m (fig. 6.b); 3) a small decrease of the aircraft speed, i.e. 0.01 m/s (fig. 6.c), this explaining the increase of the flare duration (Fig. 6.a); 4) the increase of the overshoots and transient regimes especially for the glide slope angle (fig. 6.d); 5) the flare duration and the horizontal distance covered during this stage of landing are bigger, while the appearing hump is bigger, this being an important disadvantage because, during the flight to small altitudes, the aircraft may be susceptible to accidents.

In the expressions of $\hat{P}$ and $\hat{P}^*$ the constant k has been chosen 0.5, but it is also interesting to analyze the effect of this constant's modification on the altitude and altitude deviation with respect to its nominal value. Actually, the constant k represents the weight of the matrices P_∞ and P_∞^*, while the constant (1-k) represents the weight of the matrices P and P^* in the matrices $\hat{P}$ and $\hat{P}^*$ calculated by means of the H_2/H_∞ technique. With other words, the constant k may be regarded as the weight of the H_∞ technique in the control law design, while the constant (1-k) may be regarded as the weight of the H_2 technique in the control law design. If k=1, the control law is designed only by using the H_∞ technique, while the control law is designed only by using the H_2 technique if k=0. Till now, the weights of H_2 and H_∞ techniques have been considered equal (k=1-k=0.5); now, we increase and decrease the value of constant k and we analyze which is the effect of this modification on the aircraft altitude, altitude error, speed error, and glide slope error. These characteristics, in the presence of sensor errors, are represented in fig. 7 (glide slope phase) and fig. 8 (flare phase). Analyzing the characteristics' families in fig. 7, we remark that the increase of the constant k (k=0.9) leads to the decrease of the aircraft speed with 0.6 m/s under its desired value (fig. 7.c), while the glide slope angle is insignificantly affected (fig. 7.d); in these circumstances, a lower speed means here the increase of the glide slope duration with 1 second (fig. 7.a) and of the horizontal distance covered during this first stage of landing with 70 m. On the other hand, the decrease of constant k (k=0.1) leads to the increase of the aircraft speed with 0.2 m/s (fig. 7.c), to an insignificant decrease of the glide slope duration with 0.32 seconds, and to the decrease of the horizontal distance covered during this first stage of landing with $70\,\text{m/s}\cdot 0.32\,\text{s}=22.4\,\text{m}$. Analyzing fig. 7.b, one can conclude that the altitude error is not affected by the choice of constant k, while from the second and the fourth graphics in fig. 7, one can notice that the increase of k means smaller overshoots although the differences are difficult to be visualized.

Analyzing now fig. 8 (flare phase) we remark that the exponential curve for the altitude is obtained only for k=0.5 (the weights of H_2 and H_∞ techniques are equal in the control design); increasing or decreasing the constant k, we notice that the altitude tends to zero after an important hump (fig. 8.a). During flare, the altitude must be described by null overshoot, this being achieved only for k=0.5. Moreover, the modification of k does not modify the final value of the altitude error but it dramatically increases the overshoot (fig. 8.b). On the other hand, the flare duration, the horizontal distance covered during this stage of landing, and the glide slope angle are insignificantly influenced by the modification of the weight k, but the speed error is no more zero for k=0.1 or k=0.9; thus, for k=0.1, the speed error is 0.275 m/s, while, for k=0.9, this error is even bigger (-0.95 m/s). The conclusion is clear: the only value of k for which the both stages of landing are covered well is k=0.5.

The problem of landing has also been discussed in other papers, different types of ALSs being designed [2, 3, 5, 23]. If we briefly compare our new ALS with the ones based on an Instrumental Landing System or conventional/fuzzy control of flight altitude by using the system's state [3], we remark that from the system transient regime period and overshoot point of view, the ALS based on the H_2/H_∞ technique and the dynamic inversion works slightly well. Improvement of the performance was obtained by replacing the conventional controllers with fuzzy controllers [3], but those ALSs can not be used for no-bounded exogenous signals or strongly nonlinear aircraft dynamics. The advantage of the H_2/H_∞ technique over classical control techniques is related to the applicability to problems involving multivariate systems with cross-coupling between channels, the only disadvantage being that the non-linear constraints such as saturation are generally not well-handled. Since some of the exogenous inputs, as the biases of the sensors, are usually modeled by random variables, a mixed H_2/H_∞ optimization formulation is more appropriate, taking into account that the pure H_2 and H_∞ optimization approaches deal with energy bounded exogenous signals.

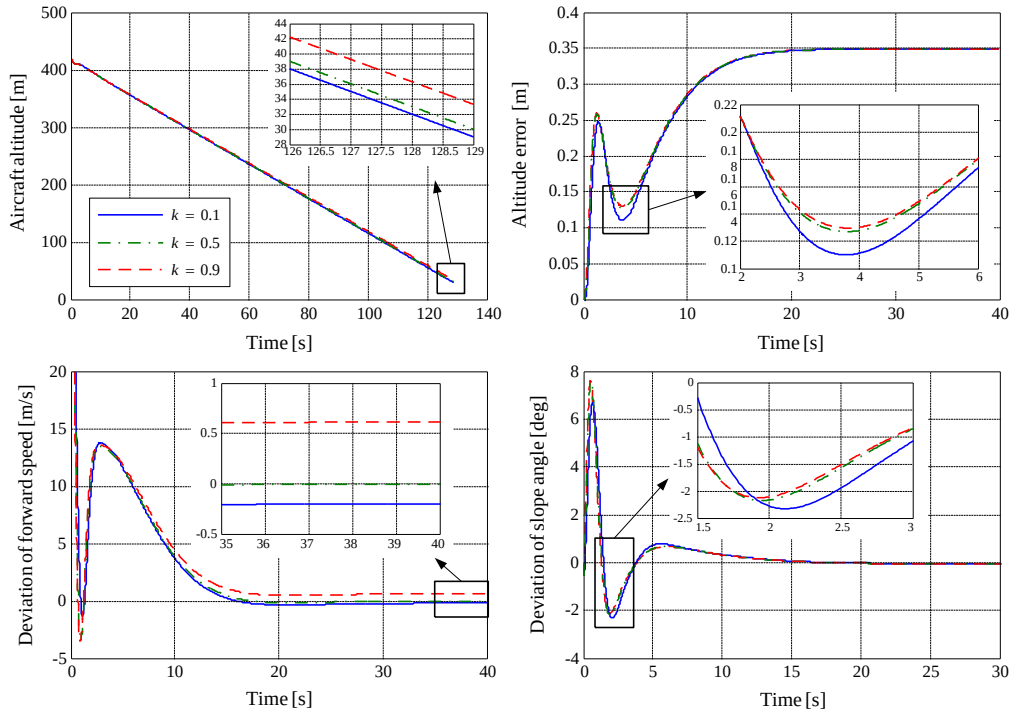

Fig. 7 Aircraft altitude and the main errors during glide slope for different values of the constant *k*

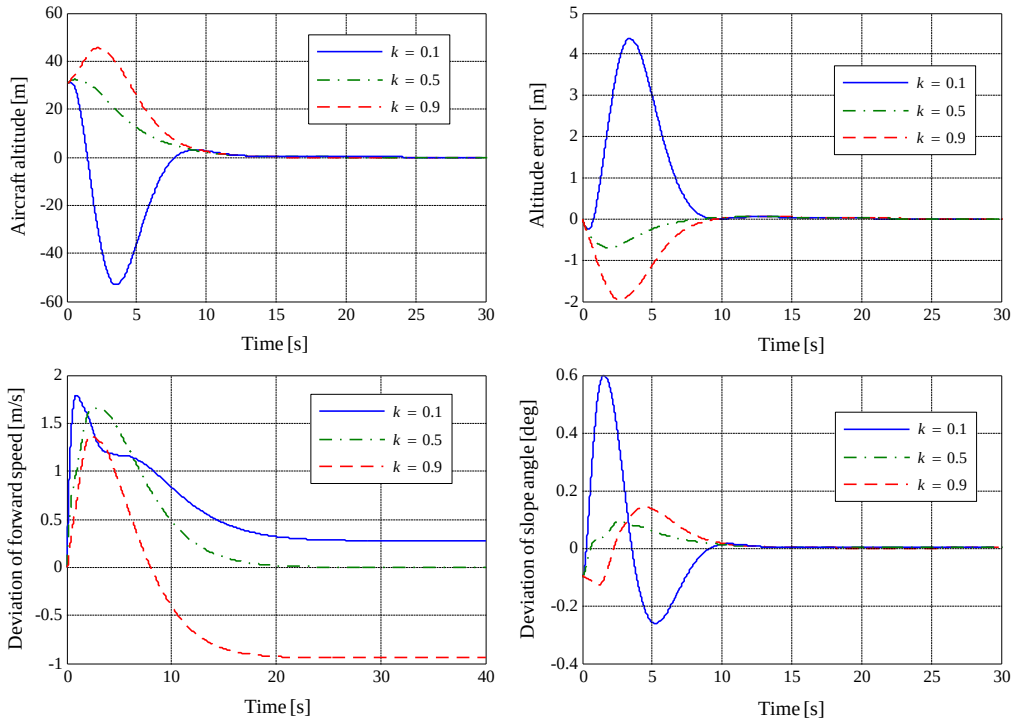

Fig. 8 Aircraft altitude and the main errors during flare for different values of the constant *k*

5. Conclusions

The purpose of this study was to design a robust automatic landing system by using the dynamic inversion, the H_2, and the H_∞ control techniques taking into consideration the sensor errors and other different disturbances; a mixed H_2/H_∞ controller based on the dynamic inversion has been obtained. It provides good precision tracking and robust stability with respect to the uncertainties caused by different disturbances and bias type signals. The ALS designed in this paper represents an improved version of the automatic landing system designed in [6] and it differs from other similar automatic landing systems from the specialty literature; our ALS is designed for the control of landing in the longitudinal (vertical) plane but, with some changes, it can also be applied to the lateral-directional motion of the aircraft during landing or other trajectories. The use of the

dynamic inversion makes our control system more general and, therefore, it can be used both for the case when aircraft dynamics is nonlinear and for the case when aircraft dynamics is linear; thus, this technique increases the generality character of our new automatic landing system. The simulation results are promising and show the robustness of the algorithm even in the presence of disturbances and sensor errors.

References

[1] Liao, F., Wang, J.L., Poh, E.K., Fault-Tolerant Robust Automatic Landing Control Design, Journal of Guidance, Control and Dynamics, vol. 28, no. 5, 2005, pag. 854-87.

[2] Lungu, R., Lungu, M., Grigorie, T. L., ALSs with conventional and fuzzy controllers considering wind shears and gyro errors. Journal of Aerospace Engineering, vol. 26, no. 4, 2012, pp. 794-813.

[3] Lungu, R., Lungu, M., and Grigorie, T. L., Automatic Control of Aircraft in Longitudinal Plane during Landing. IEEE Transaction on Aerospace and Electronic Systems, vol. 49, no. 2, 2013, pp. 1338-1350.

[4] Singh, S., Padhi, R., Automatic Path Planning and Control Design for Autonomous Landing of UAVs using Dynamic Inversion, American Control Conference Riverfront, St. Louis, MO, USA , pp. 2409-2414, 2009.

[5] Juang, J.G., Cheng, K.C., Application of Neural Network to Disturbances Encountered Landing Control. IEEE Transactions on Intelligent Transportation Systems, vol.7, no.4, 2006, pp. 582-588.

[6] Che, J., Chen, D., Automatic Landing Control using H-inf control and Stable Inversion. Proceedings of the 40th Conference on Decision and Control, Orlando, Florida, USA, 2001, pag. 241-246.

[7] Lungu, M., Sisteme de conducere a zborului (Flight control systems). Sitech Publisher, Craiova, 2008.

[8] Pashilkar, A., Sundararajan, N., Saratchhandran, P.A., Fault-Tolerant Neural Aided controller for Aircraft Auto-Landing, Aerospace Science and Technology, vol. 10, no. 1, pp. 49-61, 2006.

[9] Shue, S., Agarwal, R.K., Design of automatic landing systems using mixed H_2/H_∞ control, Journal of Guidance, Control, and Dynamics, vol. 22, pp. 103-114, 1999.

[10] Li, Y., Sundararajan, N., Saratchandran, P., Wang, Z., Robust Neuro-H_∞ controller design for aircraft auto-landing, IEEE Transactions on Aerospace and Electronic Systems, vol. 40, no. 1, pp. 158-167, 2004.

[11] Mori, R., Suzuki, S., Neural Network Modeling of Lateral Pilot Landing Control. Journal of Aircraft, no. 46, pp. 1721-1726, 2009.

[12] Lungu, R., Lungu, M., Automatic Landing Control using H-inf Control and Dynamic Inversion, Proceedings of the Institution of Mechanical Engineers Part G - Journal of Aerospace Engineering, vol. 228, no. 14, 2014.

[13] Wagner, T., Valasek, J., Digital Autoland Control Laws Using Quantitative Feedback Theory and Direct Digital Design, Journal of Guidance, Control, and Dynamics, vol. 30, no.5, pp. 1399-1413, 2007.

[14] Venkateswara, D.M., Tiauw, H.G., Automatic landing system design using sliding mode control, Aerospace Science and Technology, vol. 32, no. 1, pp. 180-187, 2014.

[15] Kumar, V., Rana, K.P., Gupta, V., Real-Time Performance Evaluation of a Fuzzy PI + Fuzzy PD Controller for Liquid-Level Process, International Journal of Intelligent Control and Systems, vol. 13, no. 2, pp. 89-96, 2008.

[16] Prasad, B., Pradeep, S., Automatic Landing System Design using Feedback Linearization Method, AIAA Infotech@Aerospace Conference and Exhibit, Rohnert Park, California, 7-10 May, 2007.

[17] Ochi, Y., Kanai, K., Automatic approach and landing for propulsion controlled aircraft by H_∞ control, Proceedings of the 1999 IEEE International Conference on Control Applications, Hawaii, pp. 997-1002, 1999.

[18] Parkinson, B., O'Connor, M., Fitzgibbon, K., Aircraft automatic approach and landing using GPS, Global Positioning System: Theory and Applications, vol. II, pp. 397-425, 1996.

[19] Zdenko, K., Stjepan, B., Fuzzy Controller Design – Theory and applications, Taylor and Francis Group, 2006.

[20] Stoica, A.M., Disturbance Attenuation and its Applications, Romanian Academy Publisher, 2004.

[21] Malaek, M., Izadi, H., Pakmehr, M., Flight Envelope Expansion in Landing Phase Using Classic, Intelligent and Adaptive Controllers, Journal of Aircraft, vol. 43, no. 1, pp. 91-101, 2006.

[22] Braff, R., Powell, J.D., Dorfler, J., Applications of GPS to air traffic control, Global Positioning System: Theory and Applications, vol. II, pp. 327-374, 1996.

[23] Fard, J.M., Nekoui, M.A., Sedigh, A.K., Amjadifard, R., Robust Multivariable Controller Design with the simultaneous $H_2/H_\infty/\mu$ for a Single Person Aircraft, International Journal of Electrical and Computer Engineering, vol. 3, no. 2, pp. 279-286, 2013.